Journal of Hydrology 610 (2022) 127938

Contents lists available at ScienceDirect

Journal of Hydrology

journal homepage: www.elsevier.com/locate/jhydrol

Impact of stormwater infiltration on rainfall-derived inflow and infiltration: A physically based surface–subsurface urban hydrologic model

Kun Zhang *, Anthony J. Parolari

Department of Civil, Construction, and Environmental Engineering, Marquette University, USA

ARTICLE INFO

Keywords:
Urban hydrology
Stormwater
Groundwater
Green infrastructure
RDII
Urban karst

ABSTRACT

The subsurface fate of stormwater infiltration enhanced by green infrastructure (GI) is unknown. GI redirects stormflows from the surface into the subsurface, which can be partitioned to evapotranspiration or baseflow, or be intercepted by buried infrastructure trenches. Stormwater that infiltrates sanitary sewer pipes is referred to as rainfall-derived inflow and infiltration (RDII) and represents a rapid pathway for infiltrated stormwater to reach receiving waters. To quantify the partitioning of infiltrated stormwater between slow and fast flows, a physically-based hydrologic model was developed integrating coupled surface–subsurface processes and urban sewer systems and applied to a sewershed near Milwaukee, WI. In this region with shallow groundwater table and leaky sanitary sewer systems, RDII accounted for 73–79% of the sanitary sewer flow volume and 21% of the sewershed water balance. Sensitivity analysis indicated that the surface direct inflow was controlled more by precipitation/evapotranspiration ratio and the subsurface infiltration was controlled more by groundwater table depth and sanitary sewer defect density. The largest effect of GI was to shift surface runoff to evapotranspiration and reduce peak flow in urban sewer systems. The volume of RDII was relatively less sensitive to GI infiltration because reductions in directly connected surface runoff were offset by increases in groundwater inflow. A moderate level of GI implementation (5–10% replacement of impervious area) reduced RDII volume by 10%, however, these changes were less than 1% of the overall water balance. On the other hand, higher levels of GI implementation (~20% replacement of impervious area) resulted in no change to RDII volume as more infiltrated stormwater was routed to the sewer system through the subsurface. This study highlights the necessity of considering the full hydrologic context of GI and balancing the runoff reduction by GI and groundwater infiltration into sewers.

1. Introduction

Infiltration-based stormwater management practices are widely implemented to mitigate urbanization impacts on hydrology. Stormwater infiltration aims to replenish soil moisture and recharge groundwater to promote slow hydrologic flowpaths, evapotranspiration and baseflow, while reducing rapid overland flow. However, infiltrated stormwater can be intercepted by buried stormwater and wastewater collection pipes, which rapidly transport flows to receiving waters (Kaushal and Belt, 2012; Bonneau et al., 2017; Pangle et al., 2022). This rapid, subsurface pipe flow has the potential to offset the benefits of stormwater infiltration (Bonneau et al., 2017). Yet, the sensitivity of urban hydrologic flowpaths to interactions between stormwater infiltration practices and buried collection system infrastructure is unknown.

Stormwater interception by buried collection system infrastructure is commonly referred to as rainfall-derived infiltration and inflow (RDII). RDII combines both direct inflows and subsurface infiltration. Direct inflows include overland flow generated on impervious surfaces that are directly connected to sanitary sewers through roof and foundation drains, storm sewer cross connections, or leaky manholes (Process 1 in Fig. 1). Subsurface infiltration includes infiltrated stormwater (Process 2 in Fig. 1) and groundwater (Process 3 in Fig. 1) that enter pipes through pipe defects (Fig. 1). RDII can be a large fraction of separate sanitary and combined sewer flows. In published studies, RDII accounted for 20–55 % of the dry weather flows in separate sewer systems (Eiswirth and Houtzl, 2006; Beheshti and Sægrov, 2018) and 14–50 % of flows in combined sewer systems (Weiss et al., 2002; Kracht et al., 2007, 2008; Prigiobbe and Giulianelli, 2009). One recent work by Pangle et al. (2022) found that RDII contributed 24–36 % of the flow by volume in sanitary sewers in Atlanta, Georgia, USA. RDII occupies system capacity, increasing the risk of sewer overflows and decreasing wastewater treatment efficiency

* Corresponding author.
E-mail addresses: kun.zhang@marquette.edu, kzhang16@connect.hku.hk, kun.zhang@marquette.edu (K. Zhang).

https://doi.org/10.1016/j.jhydrol.2022.127938

Available online 20 May 2022
0022-1694/© 2022 Elsevier B.V. All rights reserved.

(Ellis and Bertrand-Krajewski, 2010). Further, modeled RDII was found to be the largest determinant of subsurface storage relative to impervious cover and subsurface withdrawals (Bhaskar et al., 2015). Discharge of RDII can increase the subsurface storage depletion rate and reduce low flows to urban streams (Braud et al., 2013; Pangle et al., 2022). Therefore, RDII both poses operational problems for collection system utilities as well as impacts the subsurface hydrology of urbanized watersheds.

Focused stormwater infiltration using infiltration-based green infrastructure (GI) has gained traction as a stormwater control measure that enhances on-site infiltration and evapotranspiration (Fletcher et al., 2015; Avellaneda et al., 2017; Golden and Hoghooghi, 2018; Voter and Loheide, 2018; Avellaneda and Jefferson, 2020; Bell et al., 2020). For example, the City of Milwaukee plans to add 0.14 million m^3 of stormwater storage by implementing GI by 2030, which is equivalent to 58 ha of green space and would cost $2.8 million per year (City of Milwaukee, 2019). New York City has built and is planning to build over $2.9 billion GI to reduce combined sewer overflows volume (NYCDEP, 2012). Seattle also launched a surface runoff control program to control 700 million gallons of stormwater using GI by 2025 (City of Seattle, 2015). GI confers many benefits such as flood control, combined sewer overflows mitigation, water quality remediation, biodiversity enhancement, and placemaking, yet the costs and trade-offs have yet to be fully constrained (Kousky et al., 2013; Nordman et al., 2018).

One key uncertainty is the fate of infiltrated stormwater in the subsurface (Bonneau et al., 2017). Enhanced stormwater infiltration by GI has the potential to recharge groundwater, raise the groundwater table, and increase subsurface storage and baseflow (Göbel et al., 2004; Endreny and Collins, 2009; Stewart et al., 2017; Zhang and Chui, 2017; 2019; 2020; Bhaskar et al., 2018; Voter and Loheide, 2018, 2021; Choat and Bhaskar, 2020). Because of this potential impact on groundwater levels, infiltrated stormwater may increase the rate and volume of RDII. Thus, understanding the impact of GI on groundwater and RDII is critical to the design and long-term planning of stormwater infrastructure.

Several approaches have been used to quantify RDII volumes and rates, including flow monitoring (Zhang, 2007) and parametric models (Karpf and Krebs, 2011). In stormwater modeling applications, RDII is commonly assumed to be a constant fraction of precipitation or to follow a synthetic, triangular unit hydrograph (Wright et al., 2001; Mikalson et al., 2012). However, these methods may omit key feedbacks between infiltration, groundwater, and soil moisture spatio-temporal variability. These feedbacks can be captured using physically-based models, which have yet to be applied to quantify the problem of RDII. This objective frames the scope of the present work.

To quantify the impact of GI on RDII and, subsequently, the ultimate fate of infiltrated stormwater, we developed a process-based hydrologic model that couples surface and subsurface flows at the urban catchment scale. Based on the validated model, 42 artificial scenario-based simulations were performed to answer the following research questions: (1) What are the volume, rates, and sources of RDII in sanitary sewers (2) How sensitive is RDII to climate, groundwater level, and sewer system condition? And (3) Considering RDII, how does enhanced infiltration using GI affect the distribution of fast and slow stormwater flows at the catchment scale?

2. Methodology

2.1. Theory and models

Surface and subsurface hydrologic processes were simulated by solving coupled 2-dimensional shallow water equations (SWE) for the surface and 3-dimensional Richards' equation (RE) for the subsurface. The COMSOL Multiphysics package suite was used to solve these equations. COMSOL was chosen specifically because it can simulate various interactive physical processes in a flexible way. COMSOL was previously used to simulate surface–subsurface hydrologic processes at local and watershed scales in a number of studies (Chui and Freyberg, 2009; Chui and Trinh, 2016; Zhang and Chui, 2020), including applications of the coupled SWE and RE (Weill et al., 2009; Zhu et al., 2020). The conceptual model implemented here to simulate the coupled surface–subsurface processes and RDII is illustrated in Fig. 2 and described in more detail in the following sections.

2.1.1. Surface hydrologic simulation

Surface rainfall-runoff generation and runoff routing were simulated by solving 2-D SWE. The continuity of mass and momentum equations are,

$$\frac{\partial h}{\partial t} + \nabla(uh) = R - I - E \tag{1}$$

$$\frac{\partial u}{\partial t} + u\nabla(u) + g\nabla(h) + g\left(S_f - S\right) = 0 \tag{2}$$

where h is the water depth at the ground surface (m); u is the water velocity (m/s); t is time (s); R is the rate of rainfall input (m/s); I is the infiltration rate (m/s); E is the evaporation rate (m/s); and S_f and S are the friction and ground slopes, respectively (m/m).

To reduce the numerical complexity of the problem, the diffusion wave approximation was adopted to ignore the momentum losses due to acceleration and inflows (i.e., the first and second terms in Eq. (2)) (Maxwell and Miller, 2005; Downer and Ogden, 2006; Zhu et al., 2020). With this approximation, the velocity can be written as,

$$u = \frac{h^{2/3}}{n_m\sqrt{S}}\nabla(h+z) \tag{3}$$

where n_m is Manning's roughness coefficient ($s/m^{1/3}$); and z is elevation head (m).

The resulting approximate continuity equation is then,

$$\frac{\partial h}{\partial t} + \nabla\left(\frac{h^{\frac{5}{3}}}{n_m\sqrt{|S|}}\nabla(h+z)\right) = R - I - E \tag{4}$$

Eq. (4) was solved as a boundary-type partial differential equation (PDE) at the upper surface of the domain in the model. Details of the

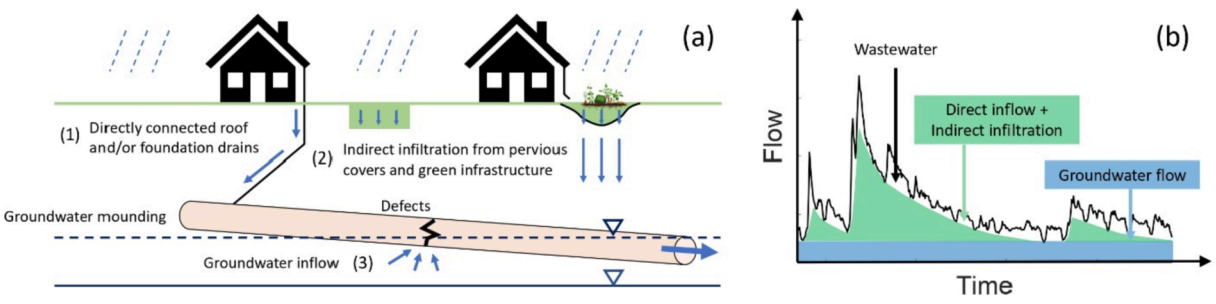

Fig. 1. (a) Potential sources of rainfall-derived inflow and infiltration (RDII) in urban sewersheds. (b) Composition of flow in sanitary sewer systems with RDII.

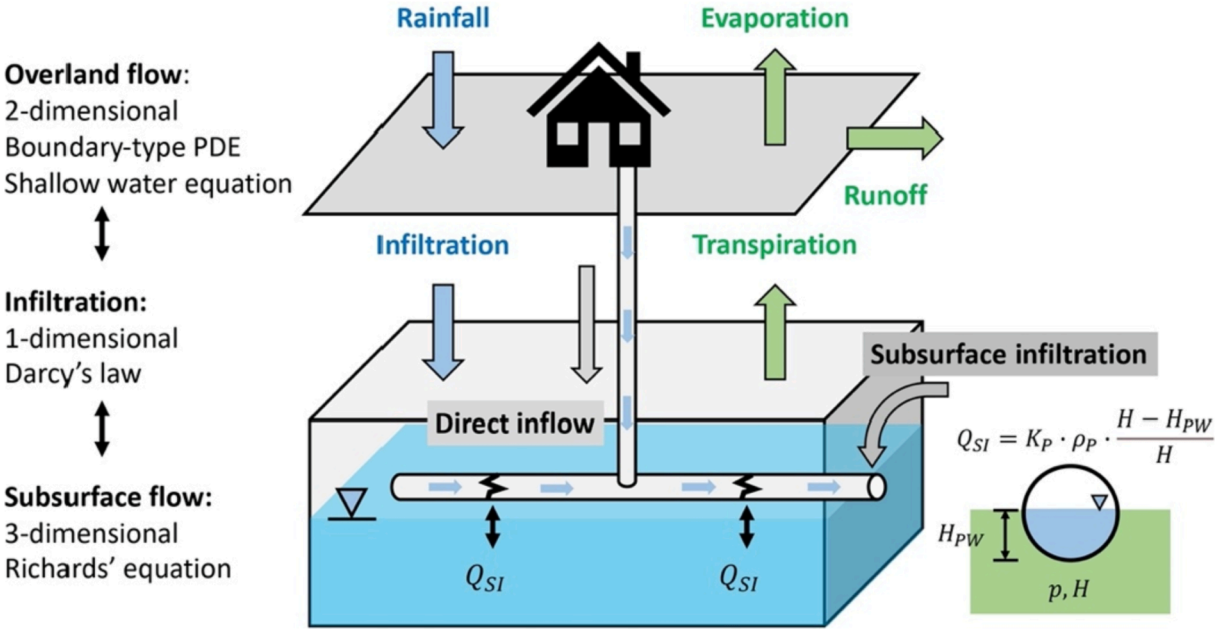

Fig. 2. Conceptual model of surface–subsurface interaction and rainfall-derived inflow and infiltration into sanitary sewers in COMSOL Multiphysics.

diffusion wave approximation can be found in supporting material (Text S1).

The stormwater drainage system was not simulated in the model. Surface runoff that was not directly connected to the sanitary sewer system was drained from the watershed using a sink term in the SWE. The sink term was activated when the runoff depth reached an allowable ponding depth of 2 cm.

2.1.2. Subsurface hydrologic simulation

The subsurface hydrologic processes were described by a 3-D Richards' equation enabled in COMSOL,

$$(C + S_e S)\frac{\partial \psi}{\partial t} + \nabla(-K(\psi)\bullet\nabla(\psi + z)) = Q \quad (5)$$

where C is specific moisture capacity (m^{-1}); S_e is the effective saturation of the soil (-); S is the storage coefficient (m^{-1}); ψ is the soil suction head (m); K is the hydraulic conductivity with respect to ψ (m/s); and Q is the source/sink term used to simulate transpiration (s^{-1}).

The RE was integrated with the SWE applied as the upper boundary condition (i.e., soil surface). The boundary condition switches between a specified flux (i.e., Dirichlet) boundary and a specified head (i.e., Neumann) depending on whether the surface was ponded or not. More specifically, the infiltration rate is specified as a constant flux equal to the rainfall intensity when the rainfall intensity is less than the surface infiltration capacity; and it is specified as a constant head equal to h when the surface is ponded. The moisture content of near-ground soils calculated by RE is fed back to SWE to calculate the infiltration capacity and infiltration rate,

$$f = K(1 + \frac{h + \psi}{L}) \quad (6)$$

where f is the infiltration capacity (m/s); h is the water depth on the ground; and L is the depth that infiltration gradient occurs (m).

Evaporation and transpiration rates (ET) from the subsurface soil were simulated together by assigning a domain sink term in the model (e.g., Q in Eq. (5)). The ET was parameterized based on soil moisture content (Eq. (7)), and it was assumed to follow an exponential decay with depth.

$$ET = \begin{cases} 1 & for \quad \theta_w \le \theta \\ \frac{\theta - \theta_w}{\theta_s - \theta_w}\alpha PET & for \quad \theta_w < \theta < \theta_s \\ 0 & for \quad \theta \le \theta_w \end{cases} \quad (7)$$

where θ, θ_s and θ_w (m^2/m^2) refer to the soil moisture content, saturated soil moisture content, and wilting point, respectively (m/m). α refers to a threshold (in the range of 0–1) which follows an exponential decay function with depth, i.e., $\alpha = \exp(d^{-1})$ with d referring to depth. A spatially uniform extinction depth was assigned, which was determined based on the rooting depth for different land covers (Jackson et al., 1996).

2.1.3. Simulation of rainfall derived inflow and infiltration

The RDII was simulated as two major components, including (1) surface direct inflow and (2) subsurface infiltration (Fig. 2). The direct inflow through connections to sanitary sewers, e.g., roof drain downspout and foundation drain connections, was simulated through assigning a boundary-type sink term in the SWE. For the baseline scenarios, 20 % of the impervious surface was directly connected to the sanitary sewers. Aerial photography demonstrated that the rooftops account for 25 % of the impervious covers and a field survey determined that 80–90 % of houses have roof drains that are directly connected to the sanitary sewers. The subsurface infiltration into the sanitary sewers was simulated by assigning line-type internal sink terms in RE. Water can infiltrate into the sewer systems if there is a positive pressure gradient toward the sewer system (Eq. (7); Fig. 2),

$$q = K_P \bullet \rho_P \bullet \frac{H - H_{PW}}{H} \quad (8)$$

where K_P refers to the coefficient representing the hydraulic conductivity between the sewer and the surrounding soil (m/s); ρ_P refers to the density of defects in sewers (-); and H and H_{PW} refer to the hydraulic pressure in the soil and the sewer, respectively (m).

Exfiltration from the sewer system to the subsurface was neglected because there was continuous infiltration of groundwater into the sanitary sewers, and exfiltration is likely limited under this condition (i.e., when the groundwater table is higher than the water level in the sanitary sewers). Wastewater flow was modeled following a sine wave function

based on the flow data during the period.

2.1.4. Simulation of enhanced infiltration by green infrastructure

Enhanced infiltration by GI was modeled by modifying the surface features. At locations where impervious cover was replaced by GI, the ground elevation was reduced by 0.5 m, the slope was re-calculated as the maximum rate of change in surface elevation on a projected 2-dimensional plane (i.e., dz/dx and dz/dy) from the center cell to its immediate neighbors (3 by 3 cell moving average). In addition, the allowable surface ponding depth was modified to represent depression storage by GI. Second, the surface Manning's n roughness coefficient (n_m) was modified to represent the change in surface friction. Third, the hydraulic conductivity (K) of the surface and near-surface layer was modified to represent the engineered soils (1 m in depth) used to enhance local infiltration by GI. These parameter changes together represent the stormwater runoff collection, detention, and enhanced infiltration by GI (Fig. 3a). Similar representation of GI has been adopted in many other spatially distributed models (Fry and Maxwell, 2017). Finally, a certain proportion of rooftop area was "disconnected", and the corresponding portion of surface runoff was routed to GI (Fig. 3b). The GI modeled in this study is most similar to vegetated infiltration-based stormwater control measures such as bioretention cells, rain gardens, infiltration trenches and grass swales that receive external surface runoff, allow surface ponding, and infiltrate stormwater into the subsurface. Other GI practices such as lined infiltration facilities, permeable pavements, and green roofs may operate differently than those modeled here.

2.2. Study area and data

2.2.1. Description of study area

The model was applied to an urban sewershed in Wauwatosa, Wisconsin, a suburb of Milwaukee (Fig. 4a). The sewershed is a medium-density residential community of 1.44 km^2 in area with 23.7 % impervious cover. The sewershed has a separate sanitary sewer system and a curb-and-gutter stormwater drainage design. The sewers are 1.5–7.6 m belowground and follow a similar gradient as the ground surface.

2.2.2. Geophysical data

The geophysical spatial data used to construct the model was obtained from multiple sources and, thus, of different spatial resolutions (i.e., between 1 and 6 m), including Digital Elevation Model (DEM), land use and land cover (LULC) data, and sanitary sewer information (Fig. 4b-d). The DEM was obtained from the 2015 LiDAR 1.5-m product (DNR, 2019), which was used to calculate surface slope. The LULC data was extracted from the NLCD 2016 1-m product (Dewitz, 2019), which was used to determine the distributions of surface K and the n_m for solving SWE, as well as the evapotranspiration (ET) extinction depth. The hydraulic conductivity, Manning's n and parameter for determining the ET extinction depth for different land covers are illustrated in the supplementary material (Table S2). In addition, the spatial information of the sanitary sewers, including the location, elevation, length and diameter of the pipes and manholes, was obtained from Metropolitan Milwaukee Sewer District (MMSD).

Apart from these spatial datasets, the groundwater table and soil profile information were extracted from the Bureau of Remediation and Redevelopment Tracking System (BRRTS) boring database of Wisconsin Department of Natural Resources (DNR) (DNR, 2020). The soils there were mainly composed of surface filling materials, silty clay, silty sand, and sandy gravel from the top down, with silty clay as the main soil type (Fig. 4e). Thus, homogeneous silty clay was selected as the soil type in the baseline simulations including model calibration and validation. The groundwater table was around 0.5–7.3 m below ground. It is hypothesized that the groundwater is connected to the Underwood Creek at the south end of the catchment (Fig. 4f). However, there could be perched shallow groundwater in the area due to the confining silty clay layer as shown in Fig. 4e. The detailed groundwater table depths and elevations at B1-B6 can be found in supporting material (Table S1).

2.2.3. Monitoring data

Hourly precipitation and sewer flow data from 2015 to 2019 was obtained from MMSD. Given that Milwaukee has a humid continental climate (i.e., Köppen climate classification Dfa), precipitation is mostly accumulated during the summer. This is reflected in the precipitation and sewer flow data shown in Fig. 5. Seasonal variations and rainfall response of RDII is apparent in the flow data. The consistent baseflow apparent in the flow data corresponds to groundwater inflow, which accounted for a significant proportion of the sewer flow and varies seasonally with the groundwater table.

The monitoring data during the summer (i.e., from July 1 to September 30) was selected for model calibration and validation. The data in 2018 was selected for calibration, and the data in 2017 was selected for validation (Fig. 5). Further simulations were forced with the climate inputs from 2018.

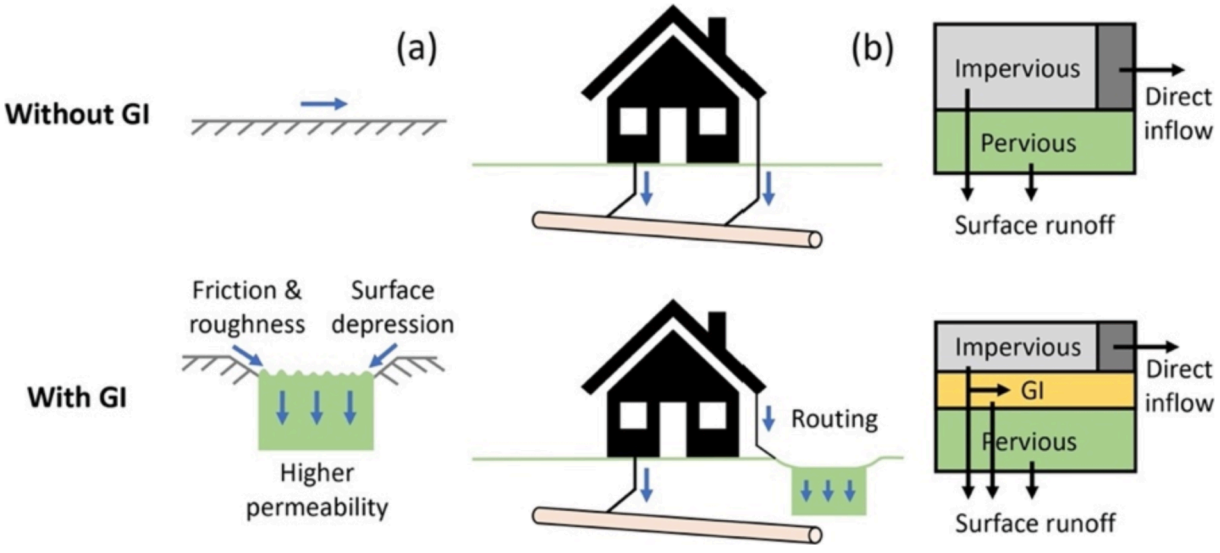

Fig. 3. Schematic showing the simulation of green infrastructure in the model through (a) modifying surface spatial features and (b) rooftop downspout disconnection and flow routing. (For interpretation of the references to colour in this figure legend, the reader is referred to the web version of this article.)

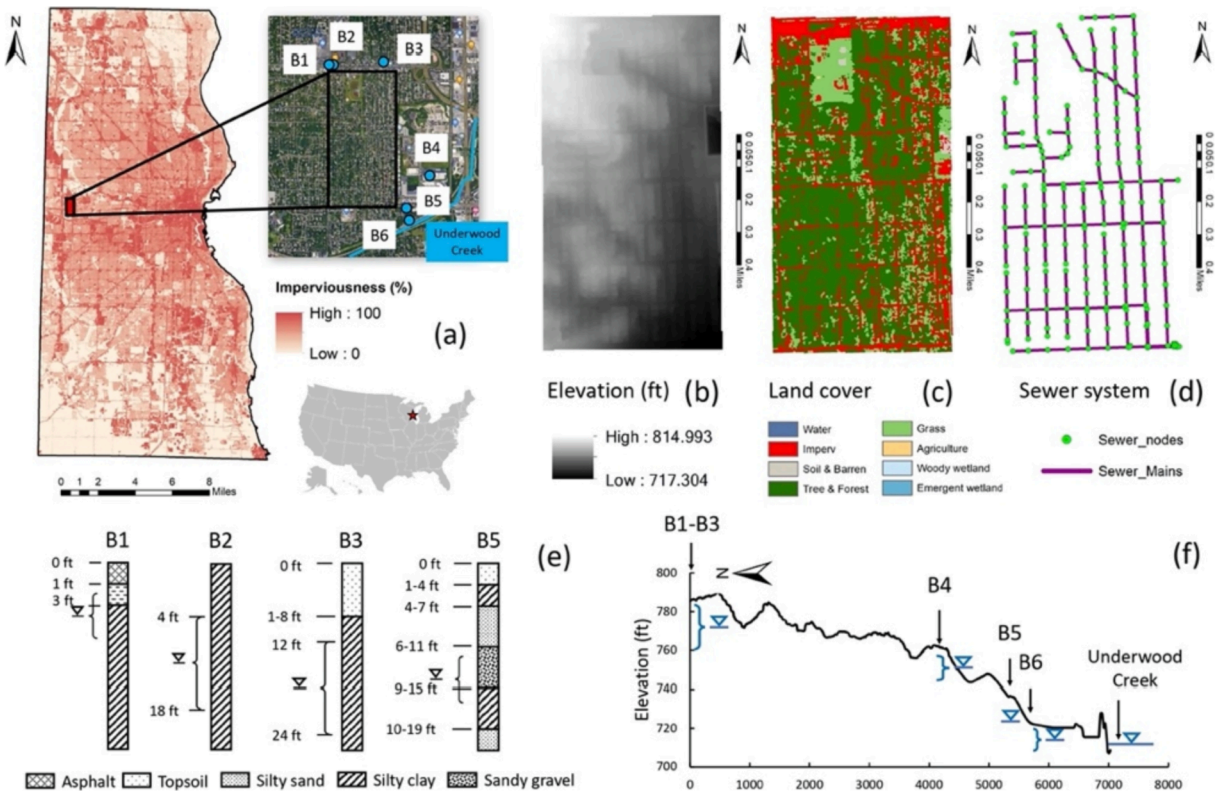

Fig. 4. (a) Geographic location of the study area within the City of Milwaukee. (b) Surface elevation distribution, (c) land cover distribution, (d) sanitary sewer system layout in the study area. (e) Soil profiles at specific locations and (f) relative elevation of groundwater levels to ground surface in the study area.

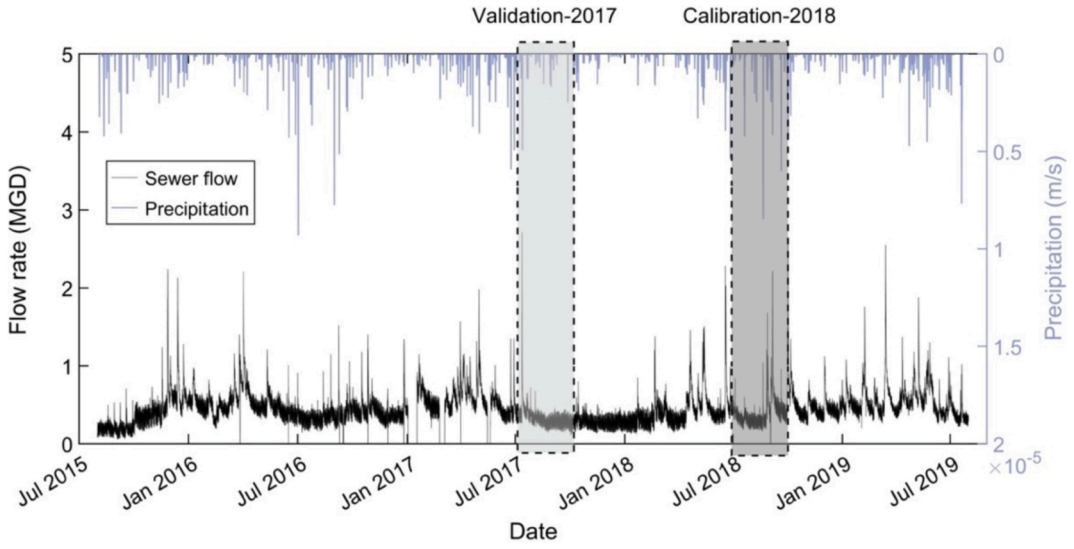

Fig. 5. Monitoring data of precipitation and sewer flow in the sewershed during the whole period. The summer (June to September) in 2018 was selected for calibration and that in 2017 was selected for validation.

2.3. Modeling settings and scenario designs

2.3.1. Domain properties

The sewershed was idealized as a 1536 m × 654 m rectangular-shaped domain for ease of model construction and simulation. The domain depth varies between 35 and 60 m. The domain was vertically discretized into a 1-m near-surface layer and a subsurface layer. A higher resolution mesh was assigned for the thin near-surface layer to provide high resolution soil moisture feedback from RE to SWE and allow customizing the hydraulic parameters for soil media of GI. Fig. 6a illustrates the domain of the sewershed. A tetrahedral mesh was constructed through user-controlled meshing sequence. With the built-in function to automatically generate physics-specific meshing schemes, a "coarser" and "extra coarse" mesh calibrated for fluid dynamics was used to discretize the near-surface and subsurface layers, respectively. In overall, the domain was discretized into 111,569 tetrahedral meshes, the overall mesh quality was good with an average mesh quality of 0.446 (range between 0 and 1 with 1 referring to perfect and > 0.1 referring to satisfactory meshing schemes). The mesh size for the near-surface and subsurface layers was 8.9–28.9 m and 11.1–44.2 m, respectively.

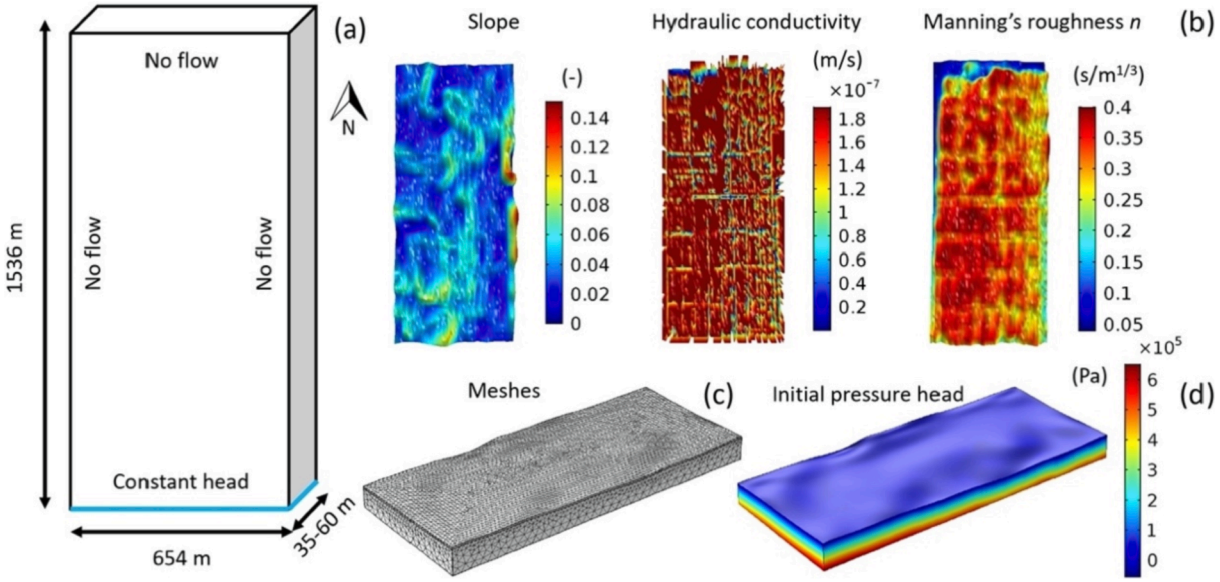

Fig. 6. Model settings of (a) model domain and boundary conditions, (b) spatial inputs including slope of ground surface, surface hydraulic conductivity, and Manning's roughness coefficient, (c) meshes, and (d) initial pressure head profile for the baseline model scenario.

The physical properties required to solve the SWE were input as spatially varied features into the model. More specifically, spatially varied slope was input based on the DEM data; and spatially varied K and n_m were input based on LULC data. A near-zero K was assigned at impervious areas, and a consistent K was assigned for areas of other land uses. The specific value of the K varied for different native soil scenarios. The Manning's roughness coefficients for different land covers were determined according to Chow (1959) and Brunner (2016). The profiles of slope, hydraulic conductivity and Manning's roughness coefficients input in the model is illustrated in Fig. 6b.

The subsurface layer of the domain was assumed to be homogeneous and isotropic. The hydraulic properties of the domain, including the water retention curve and hydraulic conductivity, were characterized using the van Genuchten function (Van Genuchten, 1980). The exact values of hydraulic conductivity and van Genuchten parameters for both the near-surface and subsurface layers vary for cases of different native soil types. Table 1 summarizes the geophysical properties in the surface and subsurface domains, and the hydraulic parameters for different soil types are illustrated in Table 2.

2.3.2. *Boundary and initial conditions*

A boundary-type partial differential equation was used to solve the SWE at the surface boundary as mentioned above. A spatially-uniform but time-dependent precipitation rate and constant evaporation rate was applied to the surface boundary. The precipitation rate was obtained from the nearest rain gauge data operated by MMSD, and the potential evapotranspiration (PET) rate was referenced from the gridded PET calculated by Ag Weather at University of Wisconsin-Madison. The rates varied among scenarios. The potential impact of vegetation and GI on PET was not simulated, but their impacts on actual ET rate can be represented in the model due to capture of soil moisture dynamics. In addition, zero gradient boundary conditions were assigned to the four sides of the boundary for SWE.

For the subsurface, no-flow boundaries were assigned to the northern, western, and eastern boundaries. Since the study area was connected to the Underwood Creek at its south and the groundwater was connected to the stream (Fig. 4f), a constant head boundary condition was used for the southern boundary based on the gage height data of the creek (Fig. 6a). The head was 2 m below ground for the baseline simulation after model calibration/validation, while it varied with the initial groundwater table depth and differ among different scenarios.

The initial surface ponding depth and its initial derivative in SWE were set as zeros. The initial condition of the RE was assigned assuming an initial groundwater table depth (Fig. 6d). Since the initial groundwater table depth and stream head at the boundary varied among scenarios, warm-up simulations were performed for each simulation with constant climatic forcing to obtain the near equilibrium state used as the initial condition. A constant precipitation and PET rate were assigned based on the average rate in the past ~ 30 years since 1991. The near equilibrium state was reached when the surface soil moisture and subsurface storage differences between time steps were within 0.05 %.

Table 1
Summary of geophysical properties of the domain.

Parameters		Values		
		Mean	Min	Max
Surface	Elevation (m)	233.3	218.6	248.4
	Slope (%)	3.0	0.0	17.5
	Manning's roughness (s/m$^{1/3}$)	–	0.01	0.37
	Imperviousness (%)	23.7		
	Hydraulic conductivity (m/s)	Near-zero for impervious areas; varied among soil type scenarios for pervious areas		
Near-surface	Depth (m)	1		
	Soil hydraulic parameters	Varied among soil type and GI scenarios		
Subsurface	Depth (m)	–	35	60
	Soil hydraulic parameters	Varied among soil type scenarios		

Table 2
Parameters used in baseline simulations and varied in model sensitivity analysis.

Groups of scenarios	Variables	Baseline	Values for sensitivity analysis				
Climatic conditions	Variations (%)	–	−80%	−40%	0 %	40%	80%
	Precipitation (mm)[1]	365	109.5	255.5	365	474.5	547.5
	PET (mm)[2]	243	365	283.9	243	226	202.8
	Precipitation/PET (-)	1.5	0.3	0.9	1.5	2.1	2.7
Groundwater conditions	Variations (%)	–	−80%	−40%	0 %	40%	80%
	Groundwater table depth (m)[3]	2.0	0.4	1.2	2.0	2.8	3.6
Sewer system conditions	Variations (%)	–	−80%	−40%	0 %	40%	80%
	Defect density of sewers (m^2/m)[4]	0.05	0.01	0.03	0.05	0.07	0.09
Surrounding soil[5]	Soil types	Silty clay	Silty clay		Loamy sand		
	Hydraulic conductivity (mm/h)	18.33	18.33		43.75		
	Saturated soil moisture (m^2/m^2)	0.489	0.489		0.39		
	Residual soil moisture (m^2/m^2)	0.05	0.05		0.049		
	α(van Genuchten) (m^{-1})	0.66	0.66		3.5		
	n(van Genuchten) (-)	1.68	1.68		1.75		
	l(van Genuchten) (-)	0.5	0.5		0.5		

Notes: [1] Precipitation was obtained from local rain gauge data requested from MMSD.
[2] PET rate was estimated from the gridded PET calculated by Ag Weather at UW-Madison.
[3] Groundwater table depth was estimated based on BRRTS boring dataset (DNR, 2020) and USGS streamflow gage data at Underwood Creek near the sewershed (USGS, 2016).
[4] Sanitary sewer density was obtained from model calibration.
[5] The hydraulic parameters of soils, e.g., hydraulic conductivity, saturated soil moisture, residual soil moisture and van Genuchten parameters α, n and l, were determined from ROSETTA (Schaap et al., 2001). Silty clay was assigned as the soil type for baseline scenarios, including for calibration/validation simulations and GI scenarios.

2.3.3. Model calibration and validation

Some parameters in the model were not available and, thus, need to be calibrated. The calibrated parameters included the depth that infiltration gradient occurs (L in Eq. (6)), sanitary sewer defect density (SDD) (ρ_P in Eq. (8)), and coefficient representing the hydraulic conductivity between the sewer and surrounding soil (K_P in Eq. (8)).

The model was calibrated through manual simulations. With other parameters unchanged (Table 2), the parameters to be calibrated were varied within a physically reasonable range in the calibration, 0.1–1 m for L, 0.001 to 0.1 m^2/m for SSD, and 10^{-7}–10^{-2} m/s for K_P. There were no specific numerical stopping criteria for the calibration, the calibration was considered finished when a reasonably good fitness between simulated and observed sewer flow was reached.

2.3.4. Simulation experiments

Several simulation experiments were performed to evaluate the sensitivity of RDII to environmental variables and parameters. The scenarios of the sensitivity analysis are shown in Table 2. More specifically, different annual precipitation/PET ratios (Precip/PET) (0.3–2.7), groundwater table depths (GWD) (0.4–3.6 m), and sanitary sewer defect densities (SDD) (0.01–0.09 m^2/m) were analyzed. The variables varied within − 80 % to + 80 % of the baselines used in or obtained through model calibration. The variables were varied through a one-at-a-time approach. When varying one variable, the other variables were kept unchanged at their baseline values. These three variables (Precip/PET, GWD, and SDD) were selected specifically because they represent climatic, geophysical, and infrastructure factors respectively and they are hypothesized to have the biggest impacts on RDII. All scenarios were run on two surrounding soil types (silty clay and loamy sand). In total, 28 simulations were performed including the base scenario. The range of Precip/PET ratio simulated in the sensitivity analysis (0.3–2.7) is representative. It covered the typical condition in most of the cities throughout the United States (Voter and Loheide, 2021). 70 % of the land worldwide falls within this range based on CRU TS monthly gridded climate dataset (Harris et al., 2020). In Milwaukee, the average Precip/PET ratio in the past 30 years was ~ 1.05 (Harris et al., 2020), which was between the baseline scenario (1.5) and the − 40 % scenario (0.9).

In addition, another 12 simulation experiments (13 including the base scenario) were performed to evaluate the impact of enhanced infiltration by GI on the volume and dynamics of RDII and, thus, the subsurface partitioning of fast and slow stormwater flows. All the simulation experiments of GI were based on the baseline scenarios as

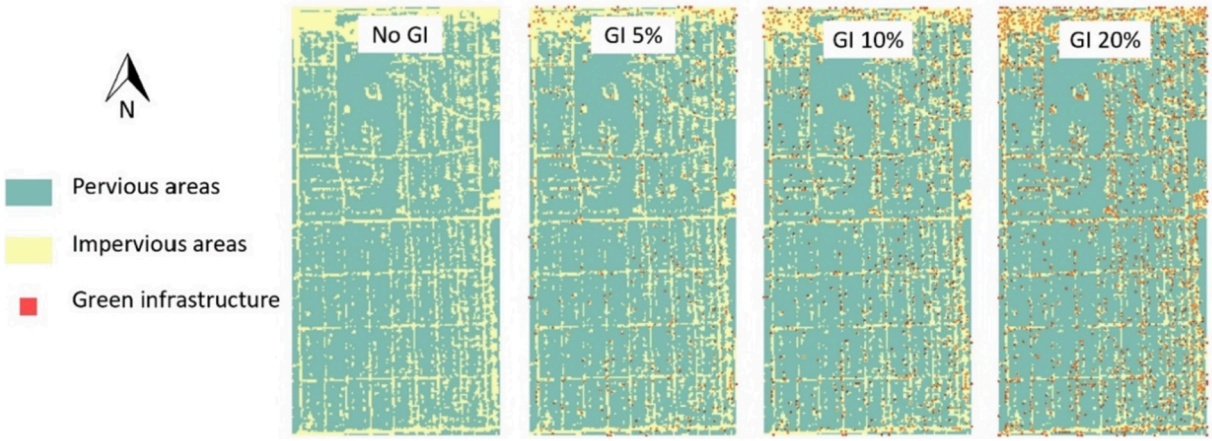

Fig. 7. Scenarios of green infrastructure in the numerical experiments. (For interpretation of the references to colour in this figure legend, the reader is referred to the web version of this article.)

mentioned above (Precip/EPT = 1.5, GWD = 2.0 m, SDD = 0.05 m^2/m and soil type of silty clay). Enhanced stormwater infiltration by GI was modeled by modifying impervious cover parameters, rooftop downspout disconnection, and runoff routing to GI as mentioned above. GI was placed at non-rooftop impervious surfaces with a uniform GI size of 6 m × 6 m. Loamy sand was selected as the media soil for GI with a hydraulic conductivity of 43.75 mm/h (Table 2). Four different GI implementation percentages, i.e., 5 %, 10 %, 15 %, and 20 % of impervious covers, and three different downspout disconnection percentages, i.e., 10 %, 20 %, and 30 %, were simulated. All the possible combinations between GI percentage and downspout disconnection percentage scenarios were simulated. As an example, Fig. 7 illustrates the spatial allocation of GI in three different GI scenarios; the GI was spatially distributed throughout the sewershed without any preference in locations. The physical meaning of GI and disconnection percentages and their impact on imperviousness can be found in supporting material (Text S2, Fig. S1).

The amount and dynamics of RDII was retrieved from the model and separated into three components, including direct inflow (DI), indirect infiltration (II), and groundwater inflow (GWI). II and GWI constitute the subsurface infiltration. The infiltration was counted as II when the groundwater table was deeper than the sewer pipes and the flow was caused by local soil saturation; in contrast, the infiltration was counted as GWI when the groundwater table was shallower than the sewer pipes.

An implicit time-dependent backward differential formula (BDF) solver with an adaptive time stepping scheme was selected. For warm-up simulations, the initial and maximum time steps were automatically determined by the software. For other simulations including model calibration/validation, an initial time step of 0.0001 day and maximum time step of 0.1 day were assigned together with a relative tolerance of 0.01. The output was extracted with a time step of $\leq$ 0.1 day with smaller time step during periods with larger errors. The computation time ranged from 30 min to 6 h per simulation.

3. Results

3.1. Model calibration and validation

The model well represents the observed sanitary sewer flow rate during the calibration and validation periods (Figs. 8, 9). In the calibration and validation periods respectively, the mean absolute error (MAE) was 0.060 and 0.046 m^3/s, and the root mean square error (RMSE) was 0.0056 and 0.005 m^3/s. During the validation period, there were fewer wet weather events, and the model was less able to simulate peak flows compared to the calibration period. The validity of the model was further tested through calculating the modeled surface and subsurface water balances; the results can be found in supporting material (Text S3, Fig. S2-S6).

3.2. Components of rainfall derived inflow and infiltration

Total RDII was dominated by GWI (Fig. 10a, b). On average, the volume of GWI was 6.6×10^4–1.2×10^5 m^3 which accounted for 55–71 % of the total sewer flow volume. DI was also a major component; the volume of DI was 1.0×10^4–2.1×10^4 m^3 which accounted for 7–18 % of the total sewer flow volume. Comparatively, indirect infiltration (II) was negligible; its volume was 4.2×10^3–1.8×10^4 m^3 and only accounted for 0.3–1 % of the total sewer flow volume (Fig. 10b). The volume of total RDII was greater than BWF. On average, the volume of RDII accounted for 73–79 % of the total sanitary sewer flow volume (Fig. 10b), and the ratio of RDII to BWF volumes was 3.0–4.3 (Fig. 10c).

GWI was larger and DI was smaller for coarse soils (loamy sand) compared to fine soils (silty clay). When surrounded by silty clay, the volumes of GWI and DI accounted for 55 ± 12 % and 18 ± 11 % of the sewer flow volume, respectively. When surrounded by loamy sand, the volumetric proportion of GWI in sewer flow increased to 71 ± 13 %, and that of DI decreased to 7 ± 6 % (Fig. 10b). Due to the dominance of GWI in RDII, the total RDII was greater for coarse soils (loamy sand) compared to fine soils (silty clay); the ratio of RDII to BWF volume was 3.0 ± 0.9 and 4.3 ± 1.6 for silty clay and loamy sand, respectively (Fig. 10c).

3.3. RDII sensitivity to climate, groundwater, and sewer defect density

The volume of RDII increased with Precip/PET ratio (Fig. 11a, b and Fig. 12a, b). When Precip/PET ratio increased from 0.3 to 2.7, the volume of RDII increased by 7.3×10^4 m^3 and 4.4×10^4 m^3 for silty clay and loamy sand surrounding soils respectively (Fig. 11a, b). Among all different components of RDII, DI was the most sensitive to Precip/PET

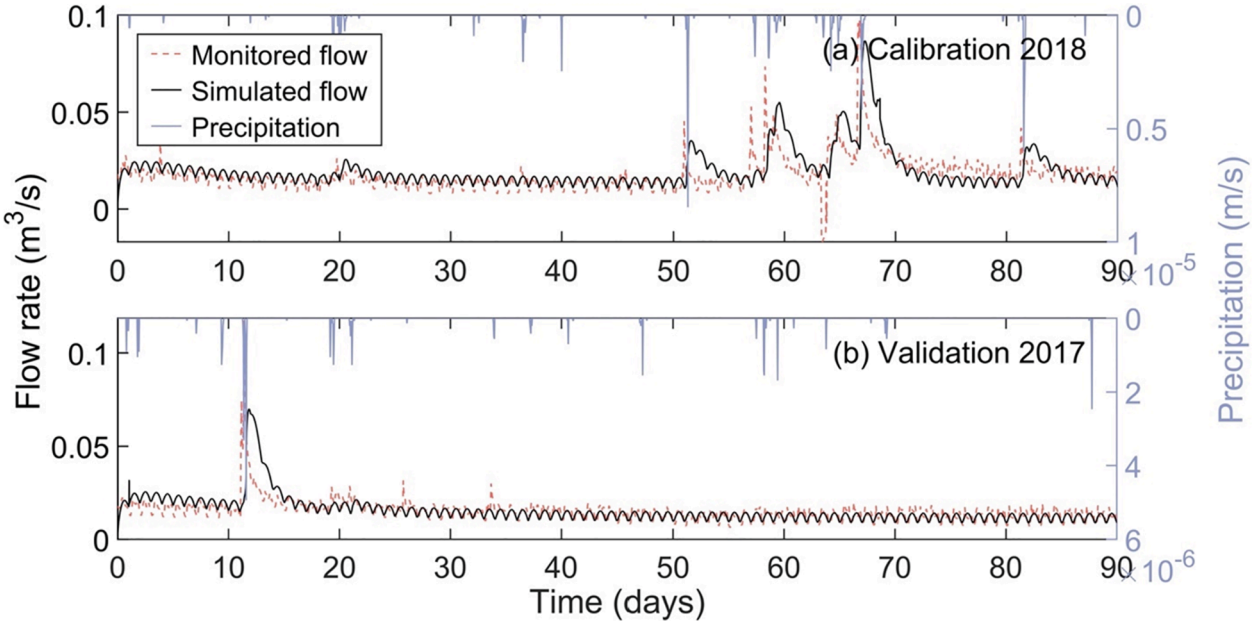

Fig. 8. Hydrographs of monitored and simulated sanitary sewer flow rates in model (a) calibration (July 1 to September 30, 2018) and (b) validation (July 1 to September 30, 2017).

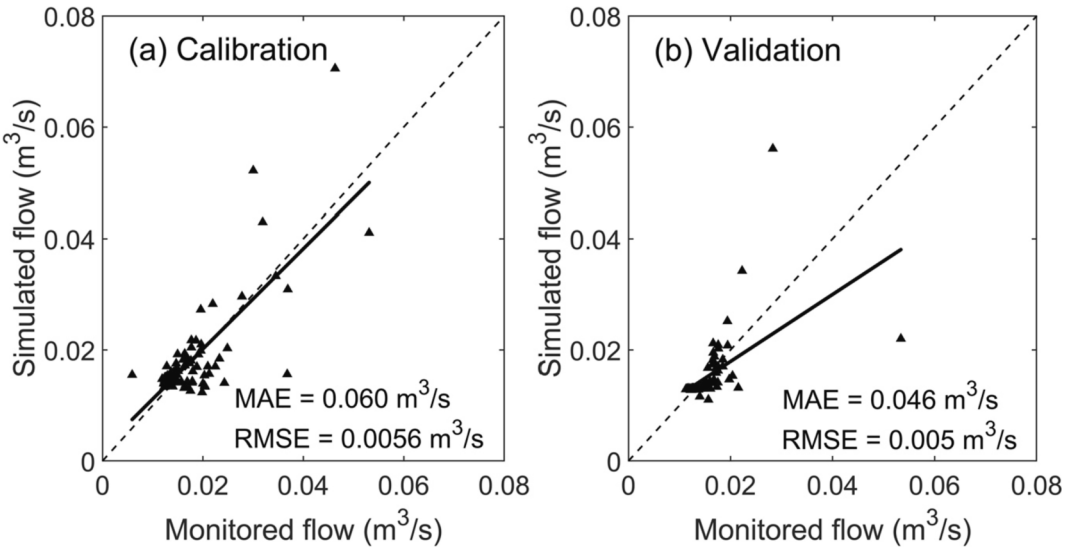

Fig. 9. Comparison of daily-averaged monitored and simulated sanitary sewer flow rates in model (a) calibration and (b) validation. MAE refers to mean absolute error. RMSE refers to root mean square error.

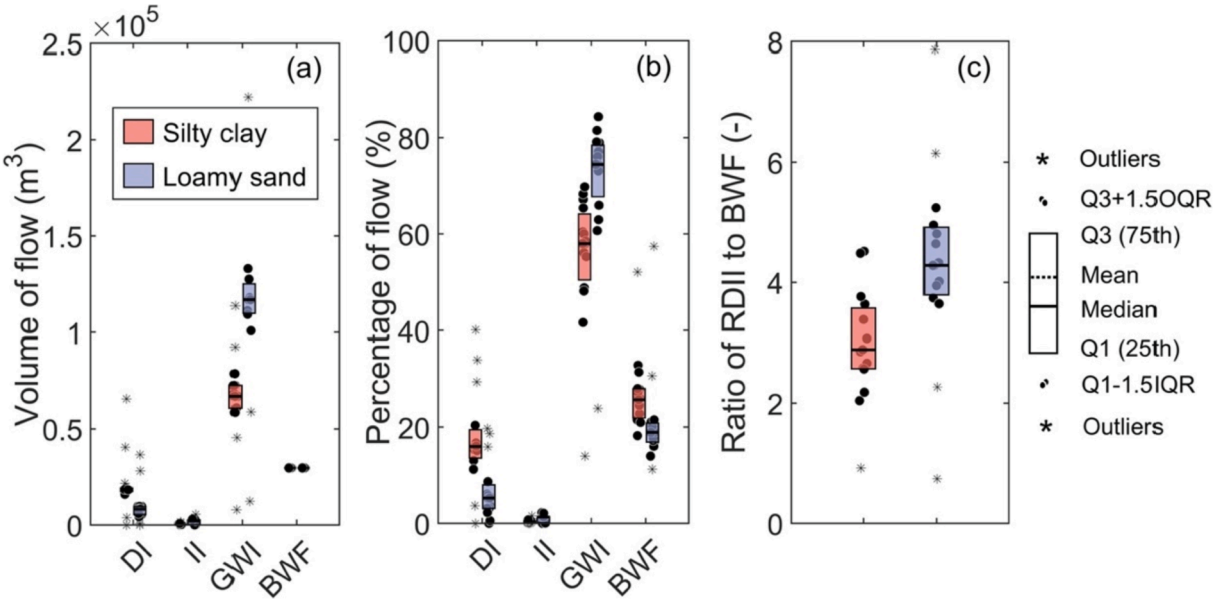

Fig. 10. Composition of rainfall derived inflow and infiltration (RDII) through simulations in terms of (a) volume, (b) percentage, and (c) ratio of RDII to base wastewater flow (BWF). DI, II, and GWI refer to direct inflow, indirect infiltration, and groundwater inflow, respectively. Each box represents the results obtained from scenarios including different precipitation/PET ratio, groundwater table depth, and sanitary sewer defect density.

ratio. When Precip/PET ratio increased from 0.3 to 2.7, the volume of DI increased by 3.7×10^4–6.6×10^5 m^3; which corresponds to a 354–380 % change with a variation of ± 80 % in Precip/PET ratio compared to the baseline scenario (i.e., Precip/PET = 1.5). GWI was not as sensitive to Precip/PET ratio. The volume of GWI only changed by 6–18 % with a variation of ± 80 % in Precip/PET (Fig. 12a, b).

The volume of GWI decreased with GWD (Fig. 11c, d and Fig. 12c, d). When GWD increased from 0.4 m to 3.6 m, the volume of RDII decreased by 2.4×10^4 m^3 and 3.5×10^4 m^3 for silty clay and loamy sand, respectively (Fig. 11c, d). Compared to other components, GWI and II were more sensitive to GWD. When GWD increased from 0.4 m to 3.6 m, the volume of GWI decreased by 2.0×10^4–3.2×10^4 m^3 (Fig. 12c, d); which corresponds to a 28–30 % change with a variation of ± 80 % in GWD compared to the baseline scenario (i.e., GWD = 2 m). With the same variation in GWD, the volume of II changed by 139–572 % (Fig. 12c, d). But it should be noted that despite its large variation in percentage, the change of II volume was very small given its small proportion of the total RDII.

The volume of RDII increased with the sewer defect density (Fig. 11e, f and Fig. 12e, f). When SDD increased from 0.01 m^2/m to 0.09 m^2/m, the volume of RDII increased by 1.1×10^5 m^3 and 2.1×10^5 m^3 for silty clay and loamy sand, respectively (Fig. 11e, f). Similar to GWD, GWI and II were also more sensitive to SDD. When SDD increased from 0.01 m^2/m to 0.09 m^2/m, the volume of GWI increased by 1.1×10^5–2.1×10^5 m^3 (Fig. 11e, f); which corresponds to a 158–180 % change with a variation of ± 80 % in *SDD* compared to the baseline scenario (i.e., SDD = 0.05 m^2/m). With the same variation in SDD, the volume of II changed by 263–427 % (Fig. 12e, f). The response of GWI to GWD and SDD dominated the RDII response due to the dominance of GWI in RDII (Fig. 11c-f).

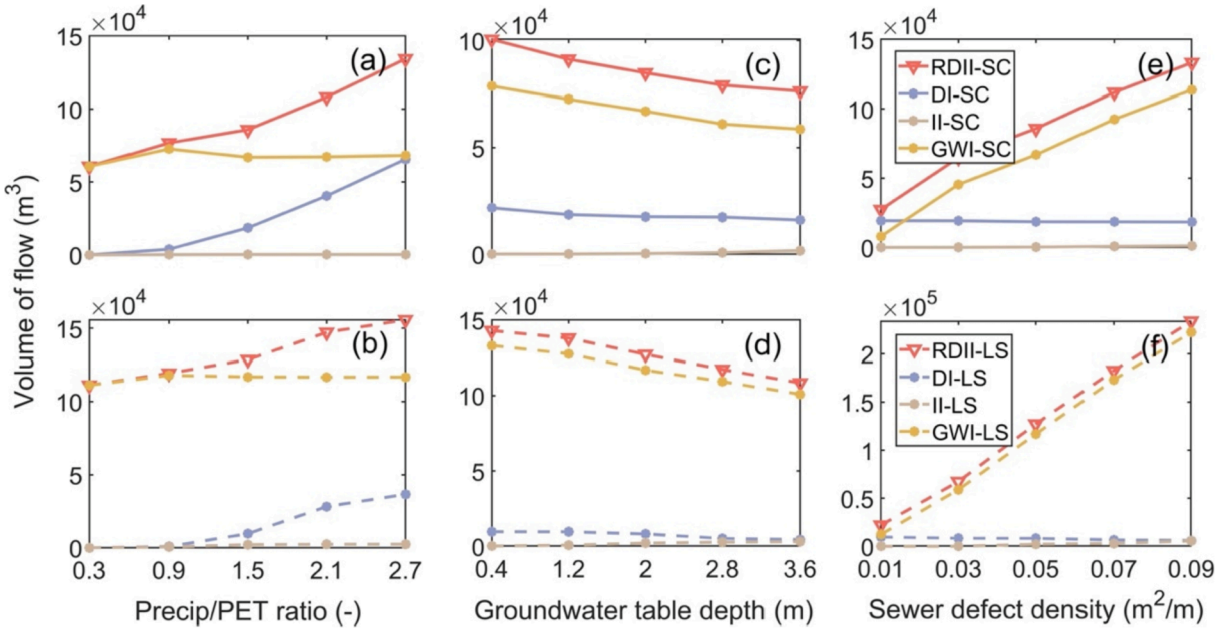

Fig. 11. Sensitivity of the volume of different components of rainfall derived inflow and infiltration (RDII) to (a, b) precipitation/evapotranspiration ratio, (c, d) groundwater table depth and (e, f) sewer defect density. DI, II and GWI refer to direct inflow, indirect infiltration, and groundwater inflow respectively; SC and LS refer to silty clay and loamy sand respectively.

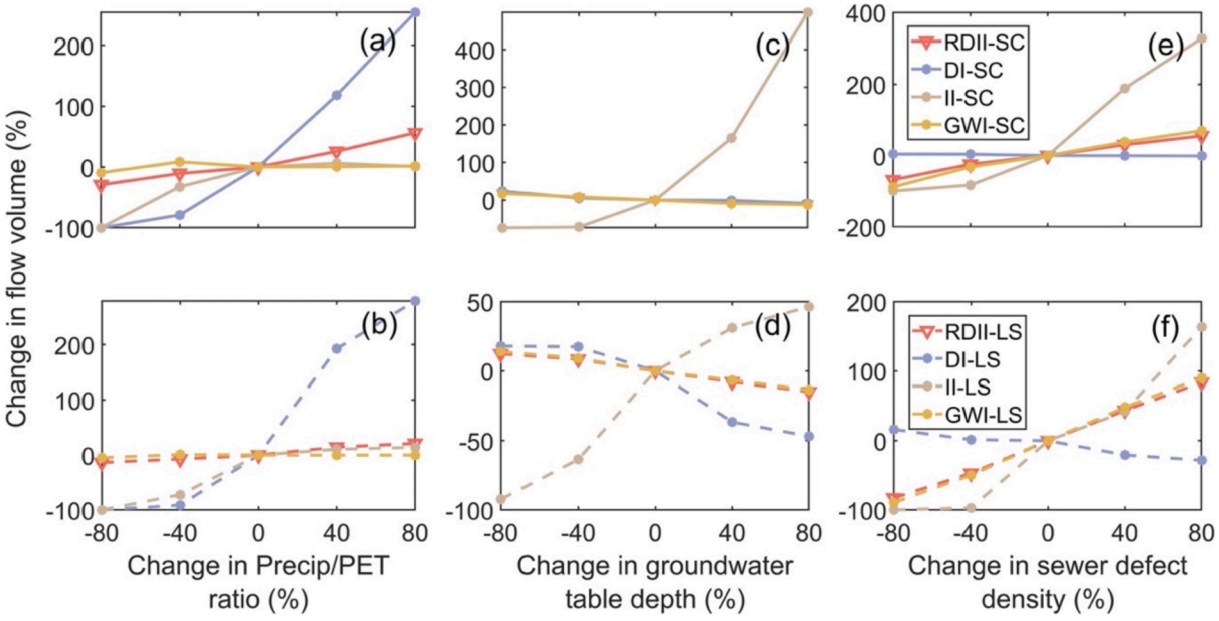

Fig. 12. Sensitivity of the percentage of different components of rainfall derived inflow and infiltration (RDII) to (a, b) precipitation/evapotranspiration ratio, (c, d) groundwater table depth and (e, f) sewer defect density. DI, II and GWI refer to direct inflow, indirect infiltration, and groundwater inflow respectively; SC and LS refer to silty clay and loamy sand respectively.

3.4. Rainfall derived inflow and infiltration after downspout disconnection and green infrastructure implementation

Fig. 13 illustrates the flow percentiles (Q10, Q50 and Q90) retrieved from the flow duration curves (FDCs) of RDII under different GI and downspout disconnection scenarios (Fig. S7-S8). GI and downspout disconnection decreased the high flows (Q90) of RDII; and with more impervious cover treated or replaced by GI, the high flows were lower. When there was no GI and downspout disconnection, the mean Q90 of RDII was 0.02 m^3/s. While, the mean Q90 of RDII was decreased to 0.014 m^3/s and 0.013 when 10 % and 30 % of downspout was disconnected (Fig. 13a); and the mean Q90 of RDII was decreased to 0.015 m^3/s and 0.013 m^3/s when 5 % and 20 % of impervious area was replaced by GI (Fig. 13b).

GI and downspout disconnection increased intermediate (Q50) and low (Q10) flows of RDII; and with more impervious cover treated or replaced by GI, the low flows were higher. When there was no GI and downspout disconnection, the mean Q10 of RDII was 0.006 m^3/s, and the mean Q50 of RDII was 0.009 m^3/s. While, when 10 % and 30 % of downspout was disconnected or when 5 % and 20 % of impervious area was replaced by GI, the mean Q10 of RDII was increased to 0.007 m^3/s and 0.008 m^3/s, and the mean Q50 of RDII was increased to 0.009 m^3/s

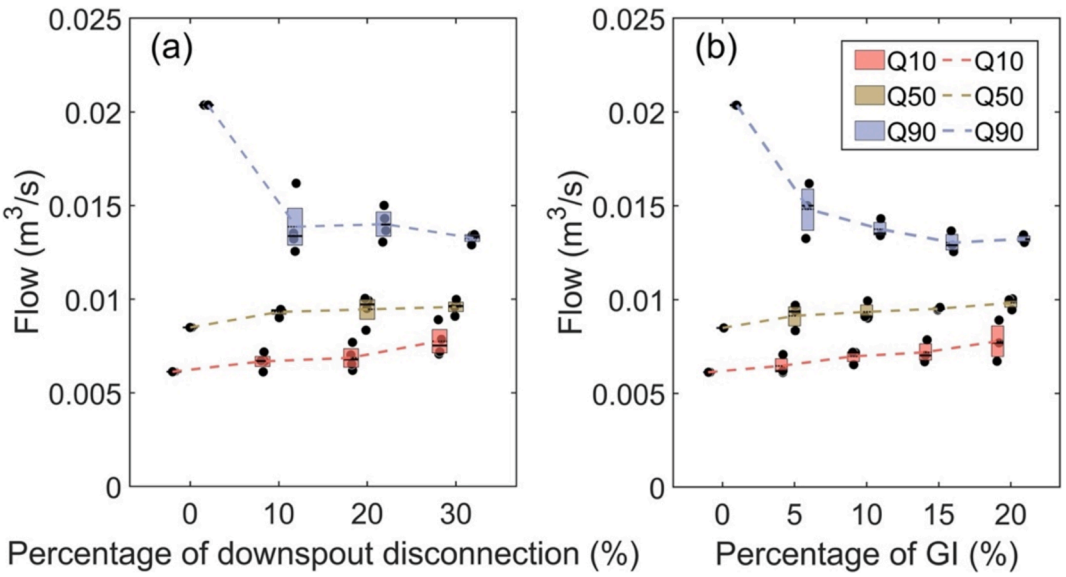

Fig. 13. Impact of green infrastructure (GI) and rooftop downspout disconnection on the flow percentiles retrieved from flow duration curves of rainfall derived inflow and infiltration (RDII). Q10, Q50 and Q90 refer to low, intermediate, and high flow rates with exceedance probability of 10 %, 50 % and 90 %. (For interpretation of the references to colour in this figure legend, the reader is referred to the web version of this article.)

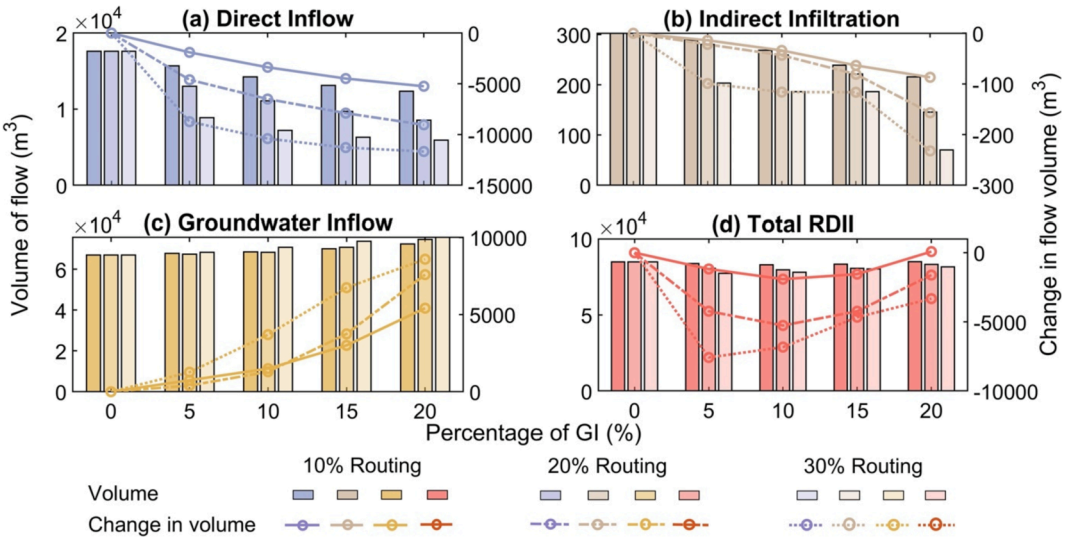

Fig. 14. Impact of green infrastructure (GI) and rooftop downspout disconnection on the volumes of different components of rainfall derived inflow and infiltration (RDII). (a) Direct inflow; (b) Indirect infiltration; (c) Groundwater inflow; (d) Total RDII. (For interpretation of the references to colour in this figure legend, the reader is referred to the web version of this article.)

and 0.01 m^3/s (Fig. 13a and b).

Fig. 14 illustrates the total and components of RDII under different GI and downspout disconnection scenarios. With more impervious cover replaced by GI, there was less DI and more GWI. When 10 % of the DI was disconnected and routed to GI, and when 5 % of impervious area was replaced by GI, the volume of DI was decreased by 1.9×10^3 m^3, and the volume of GWI was increased by 7.4×10^2 m^3. While the decrease of DI and increase of GWI raised to 5.2×10^3 m^3 and 5.4×10^3 m^3 respectively when 20 % impervious area was replaced by GI (Fig. 14a, c).

The volume of RDII responded to the areal percentage of GI in a nonlinear fashion due to the contrasting responses of DI and GWI to GI (Fig. 14d). When a small percentage of impervious cover was converted to GI (i.e., 5–10 %), the volume of RDII decreased. In contrast, when more impervious cover was converted to GI (>10%), RDII volume was reduced less (Fig. 14d). Using the scenario with 30 % downspout disconnection as an example, when 5 % of impervious area was replaced by GI, the volume of RDII was decreased by 7.6×10^3 m^3. When 20 % of impervious area was replaced by GI, the volume of RDII was decreased 3.3×10^3 m^3 (Fig. 14d). Due to the nonlinearity of total RDII to GI, there was an area percentage of GI that minimized RDII. In this sewershed, replacing 5–10 % of imperviousness to GI showed the highest efficiency in reducing RDII due to the balance between reducing DI and increasing GWI (Fig. 14d).

3.5. *Water balance sensitivity to green infrastructure implementation*

The water balance fraction for each outflow, surface runoff, RDII, ET, and subsurface outflow, were defined as a percentage of precipitation plus the change in subsurface storage (Fig. 15a). In terms of water balance fraction, surface runoff and ET were most sensitive to GI implementation and rooftop downspout disconnection. With a Precip/PET

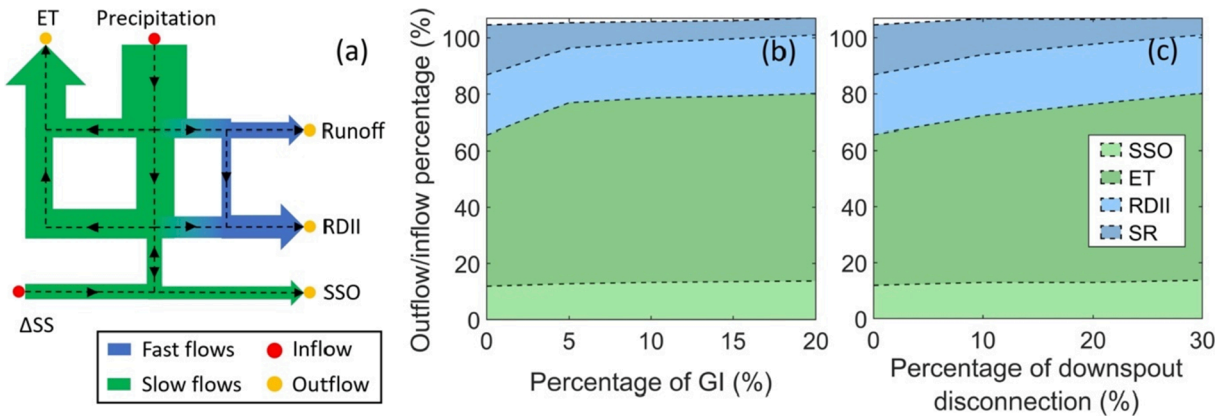

Fig. 15. (a) Surface-subsurface integrated water balance and (b-c) outflow/inflow percentage with (b) different impacts of green infrastructure (GI) (5–20 % replacement of imperviousness; 30 % rooftop downspout disconnection) and (c) rooftop downspout disconnection (10–30 %; 20 % replacement of imperviousness). Inflow includes precipitation and change in subsurface storage (ΔSS); outflow includes surface runoff (SR) (removed direct inflow of RDII), rainfall-derived inflow and infiltration (RDII), evapotranspiration (ET), and subsurface outflow out of the watershed (SSO). (For interpretation of the references to colour in this figure legend, the reader is referred to the web version of this article.)

ratio of 1.5 and no GI and downspout disconnection, slow outflows comprised 65 % of the water balance, including 12 % subsurface outflow and 53 % evapotranspiration. Fast outflows comprised 38 %, with 21 % partitioned to RDII and 17 % partitioned to surface runoff. With 20 % of imperviousness replaced by GI and 30 % rooftop downspout disconnection, slow outflows comprised 80 % of the water balance, including 14 % subsurface outflow and 66 % evapotranspiration. Fast outflows comprised 27 %, with 21 % partitioned to RDII and 6 % partitioned to surface runoff (Fig. 15b, c). Therefore, the largest impact of GI was to increase ET and decrease surface runoff, with a relatively smaller increase in subsurface outflow and no change in RDII. The maximum change in RDII was only 1 % of the water balance, although RDII itself decreased 10%.

4. Discussion

4.1. Volume and composition of rainfall derived inflow and infiltration

RDII was a major component of sewer system flow volume and the sewershed water balance. The volume of RDII was 73–79 % of the total sanitary flow volume and it was 3.0–4.3 times the dry weather wastewater flow volume during the summer (July–September). The proportion of flow attributed to RDII in this study was greater than most of the observations reported in existing literature. For example, various studies demonstrated that the volume of RDII was 14–50 % of sewer flow volume in combined sewer systems (Weiss et al., 2002; Kracht et al., 2007, 2008; Prigiobbe and Giulianelli, 2009); and its volume was 0.3–1.2 times of the dry weather wastewater flow volume for separate sewer systems (Eiswirth and Houtzl, 2006; Beheshti and Sægrov, 2018; Pangle et al., 2022). RDII was 21% of the sewershed water balance, which is the first estimate of this fraction as far as the authors are aware.

RDII was mainly composed of GWI. This was attributed to the shallow groundwater table in the study area (~2 m below ground). In areas with a shallow groundwater table, infiltrated stormwater can recharge the groundwater more quickly (Zhang and Chui, 2017; Bhaskar et al., 2018) and a larger amount of groundwater can infiltrate into the sewer system pipes. The groundwater table is shallow in this region within the vicinity of the sanitary sewer pipes (0.5–7.3 m below ground) (Fig. 4e, f) (DNR, 2020); and the near-surface soils in the region are silty clay (DNR, 2020) which are prone to perched groundwater near the surface or directing infiltrated stormwater quickly to higher conductivity pipe trenches. Existing studies also reported the dominance of GWI in RDII and sewer flows. Kracht et al. (2007) performed $^{18}O/^{16}O$ isotope test in the field and estimated the amount and dynamics of GWI through isotope composition analysis. They found that GWI contributed approximately 39 % of the sanitary sewer flow. Karpf et al. (2007) estimated RDII using a regression model and they found that subsurface infiltration, i.e., including II and GWI, contributed 74 % of the total RDII. Pangle et al. (2022) estimated the RDII in 4 urban watersheds in Atlanta, Georgia through time series analysis, and they found that GWI contributed ~ 81–88 % of the total RDII. In sewersheds with higher defect densities, e.g., 0.1–2.17 m^2/m observed in Korea, greater dominance of GWI can be potentially observed (Han and Song, 2017). Contrasting observations were obtained in other studies, possibly due to differences in geophysical conditions (e.g., groundwater table and soil conditions) and sewer system conditions (e.g., designs of sewer system laterals and defect conditions on sewer system pipes). For example, Jiang et al. (2019) studied one residential subdivision and found that DI from residential weeping tiles contributed 85 % of RDII. Pawlowski et al. (2014) investigated a larger residential area (116 houses) served by separated sanitary sewers in Columbus, Ohio. They found that DI from roof drains and laterals contributed ~ 98 % of RDII, and the contribution of GWI was negligible. Tan et al. (2019) estimated the amount of RDII based on flow monitoring data, and they found comparable proportions of quick, intermediate, and slow flows and identified RDII as the main contributor.

4.2. Impact of stormwater infiltration and sewer system interception on the distribution of fast and slow flows

The modeling results presented here suggest that the partitioning of water infiltrated through GI between evapotranspiration, groundwater recharge, and RDII, impacts how effective GI is at redirecting stormwater flows from fast to slow pathways. Disconnecting rooftop downspouts and routing to GI can reduce urban hydrologic impact, decrease fast surface runoff and increase slow flows such as ET. With 20 % of imperviousness replaced by GI and 30 % of downspout disconnection, the percentage of slow outflows (e.g., subsurface outflow and evapotranspiration) increased by 15 % (from 65 % to 80 %), and the percentage of fast outflows (e.g., surface runoff and RDII) decreased by 11 % (from 38 % to 27 %). The gap in between was caused by numerical errors in simulations. The percentage of ET in the water balance was consistent with the climatology of Wisconsin (Sun et al., 2008; Voter and Loheide, 2018).

Similar relative change in water budget partitioning by GI can be expected in areas with similar climatic conditions (i.e., Precip/PET ratio

close to 1), but may be different in drier or wetter climates (Voter and Loheide, 2021). For more arid areas or drier periods with lower Precip/PET ratios, although there is smaller hydrologic input to GI, the relative change in water budget partitioning by GI may be greater because a larger proportion of enhanced infiltration by GI can be lost via ET and less can be routed as quick flow into the system (Lizárraga-Mendiola et al., 2017; Ebrahimian et al., 2019). For wetter areas or periods with higher Precip/PET ratios, the relative change in water budget partitioning by GI may be less significant because more water can be transformed as runoff due to high runoff loads and more water can be discharged into the system without being well evaporated or transpired in the subsurface (Sohn et al., 2019). Retention ability and hydraulic residence time could be a key factor determining the GI impact on water balance (Stewart et al., 2017). Thus, varied hydrologic response can be also expected for other types of GI such as permeable pavements, green roofs, and lined GI with underdrains. Although the surface permeability of permeable pavements can be higher, enhanced infiltration and ET may be lower because they are normally not designed to receive external runoff and do not allow ponding. Green roofs and lined infiltration-based GI with underdrains can retain and delay the runoff but are normally inefficient in runoff volume reduction and rainwater redistribution due to shorter hydraulic residence time (Eger et al., 2017). And they are not connected to groundwater and would not impact RDII.

By decreasing DI entering the sewer systems, GI mitigated the peak sewer flows and can contribute to reducing the risk of sanitary or combined sewer overflows (Lucas and Sample, 2015; Ghodsi et al., 2021). The exact effect of GI on mitigating sewer overflows needs more explorations because the rainfall events in the simulation period were smaller than 2-year return period; Overflow events were normally triggered by major rainfall events (Sandoval et al., 2013; Jean et al., 2018), during which the effect of GI in reducing peak flows are expected to be lower (Chui et al., 2016). In addition, GI may not significantly reduce the total volume and percentage of RDII in urban water balances as the reduction in DI can be offset by the increase in GWI. Some infiltrated stormwater can raise the groundwater table (Göbel et al., 2004; Endreny and Collins, 2009; Zhang and Chui 2017; Bhaskar et al. 2018; Zhang and Chui, 2020) and be redistributed into RDII, especially when disconnecting and routing too much runoff to GI (e.g., $>$ 20 % replacement of impervious cover). This unintended consequence may partially offset the benefit provided by GI in transforming fast flows into slow pathways on the surface.

The situations considered in this study are close to extreme scenarios. In practice, the benefit of fast-to-slow flow redistribution by GI and downspout disconnection may not be easily offset due to the facts that 1) it is highly infeasible to replace $>$ 20 % of impervious surfaces with GI from the perspectives of economics and land use planning; and 2) not every sewer system is comparably leaky and with shallow groundwater tables within the vicinity of the pipes. However, the modeling results highlight the necessity of considering the full hydrologic context of GI, and balancing the runoff reduction by GI and groundwater infiltration into sewers.

4.3. Limitation

As a preliminary attempt to simulate catchment-scale RDII within a physically-based modeling framework, several necessary simplifications were made. Specifically, a spatially uniform sanitary sewer defect density was used to represent the deterioration condition and the porosity of the sewers (Karpf and Krebs, 2011; Fung and Babcock, 2020). In practice, however, the pipe condition will be highly heterogeneous (Okwori et al., 2021) since the structural deterioration of sewer pipes can be influenced by various internal and external factors such as the installation and maintenance methods, sewer pipe materials and diameter, design of connections, flow rate and pressure, groundwater level, soil type and hydraulics (Davies et al., 2001; Ana et al., 2009; Malek Mohammadi et al., 2020) which can be highly heterogeneous spatially (Elachachi et al., 2012; Herrmann et al., 2018). In addition, the distribution of urban trees can also add external heterogeneity to the structural deterioration condition of sewer pipes (Randrup et al., 2001; Torres et al., 2017). For more practical representation, this heterogeneity may need to be considered in the model. Exfiltration from sanitary sewers was neglected. Although the impact can be minimal in this study area due to dominance of subsurface infiltration over exfiltration, exfiltration can be a significant part of the hydrologic processes and should better be considered when the groundwater table is not as shallow (Selvakumar et al., 2004). In addition, a constant water level in the sanitary sewer pipes was assumed, and the flow routing in sanitary sewers was not modeled. This assumption may affect the dynamics and time delay of RDII captured at the outlet of the catchment. For improvement, the model can be integrated with a hydro-dynamic model to simulate sanitary sewer hydraulics by solving the Saint-Venant equations. For example, Peche et al. (2017) coupled a groundwater inflow model (i.e., OpenGeoSys) with a hydro-dynamic model (i.e., HYSTEM) to simulate pipe leakage into the subsurface.

5. Conclusion

Stormwater infiltration can transform fast surface stormflow into slow subsurface flow toward restoring the urban hydrologic cycle. However, the subsurface pathways of infiltrated stormwater are unknown; these slow subsurface flows can be collected by buried stormwater/wastewater systems, transformed back into quick flow, referred to as rainfall-derived inflow and infiltration (RDII). A physically based integrated hydrologic model was built and validated to simulate RDII. Based on the validated model, the composition of RDII into sanitary sewers was evaluated, and the partitioning of infiltrated stormwater by GI between slow and fast flows was quantified.

In areas of shallow groundwater table and leaky sanitary sewer systems like this study area, RDII can be a major flow component in sanitary sewer systems and of the water balance. RDII was dominated by groundwater inflow and the volume of RDII was 73–79 % of the sanitary sewer flow volume and 21 % of the overall water balance during the summer. Among different environmental variables, direct inflow was most sensitive to precipitation/evapotranspiration ratio; while, in contrast, subsurface infiltration was most sensitive to groundwater table depth and to the sanitary sewer defect density.

GI can restore natural hydrologic cycle through shifting surface runoff into evapotranspiration; and by decreasing direct inflow into sanitary sewer systems, GI can reduce the peak flows and the risk of sanitary sewer overflows. However, GI and rooftop downspout disconnection showed limited effect on reducing RDII volume because reductions in directly connected surface runoff were offset by increases in groundwater inflow into sanitary sewer systems. With a moderate level of GI (5–10 % replacement of imperviousness), RDII was reduced by 10 %, which, however, was only 1 % of the overall water balance. With a higher level of GI implementation (~20 % replacement of imperviousness), RDII was not reduced because more groundwater inflow entered the system from the subsurface.

Due to the substantial amount of RDII entering the sanitary sewer systems and the potential partitioning of infiltrated stormwater by GI into fast flows, this study highlights the necessity of considering the full hydrologic context of *GI* and balancing the runoff reduction by GI and groundwater infiltration into sewers.

CRediT authorship contribution statement

Kun Zhang: Conceptualization, Methodology, Software, Formal analysis, Investigation, Data curation, Writing – original draft, Visualization. **Anthony J. Parolari:** Resources, Validation, Writing – review & editing, Supervision, Project administration, Funding acquisition.

Declaration of Competing Interest

The authors declare that they have no known competing financial interests or personal relationships that could have appeared to influence the work reported in this paper.

Acknowledgements

The authors acknowledge the National Science Foundation Industry/University Cooperative Research Center on Water Equipment & Policy located at the University of Wisconsin Milwaukee (IIP-1540032) and Marquette University (IIP-1540010) for supporting this project, and Spencer Sebo and Dr. Walter McDonald for collecting and summarizing the sanitary sewer flow and digitalized sewershed data. Special thanks are extended to Matt Magruder from Milwaukee Metropolitan Sewer District (MMSD) and the mentors of the project including Benjamin D. Benningholff, Peter C. Wood and Jacob L. Zimmerman from Wisconsin Department of Natural Resources (DNR), Joe Burke from WattsWater, and Nate Qualls from NewWater.

Appendix A. Supplementary data

Supplementary data to this article can be found online at https://doi.org/10.1016/j.jhydrol.2022.127938.

References

Ana, E., Bauwens, W., Pessemier, M., Thoeye, C., Smolders, S., Boonen, I., De Gueldre, G., 2009. An investigation of the factors influencing sewer structural deterioration. Urban Water J. 6 (4), 303–312. https://doi.org/10.1080/15730620902810902.

Avellaneda, P.M., Jefferson, A.J., Grieser, J.M., Bush, S.A., 2017. Simulation of the cumulative hydrological response to green infrastructure. Water Resour. Res. 53 (4), 3087–3101. https://doi.org/10.1002/2016WR019836.

Avellaneda, P.M., Jefferson, A.J., 2020. Sensitivity of streamflow metrics to infiltration-based stormwater management networks. e2019WR026555 Water Resour. Res. 56 (7). https://doi.org/10.1029/2019WR026555.

Beheshti, M., Sægrov, S., 2018. Sustainability assessment in strategic management of wastewater transport system: case study in Trondheim, Norway. Urban Water J. 15, 1–8. https://doi.org/10.1080/1573062X.2017.1363253.

Bell, C.D., Wolfand, J.M., Panos, C.L., Bhaskar, A.S., Gilliom, R.L., Hogue, T.S., Hopkins, K.G., Jefferson, A.J., 2020. Stormwater control impacts on runoff volume and peak flow: A meta-analysis of watershed modelling studies. Hydrol. Process. 34 (14), 3134–3152. https://doi.org/10.1002/hyp.13784.

Bhaskar, A.S., Welty, C., Maxwell, R.M., Miller, A.J., 2015. Untangling the effects of urban development on subsurface storage in Baltimore. Water Resour. Res. 51 (2), 1158–1181. https://doi.org/10.1002/2014WR016039.

Bhaskar, A.S., Hogan, D.M., Nimmo, J.R., Perkins, K.S., 2018. Groundwater recharge amidst focused stormwater infiltration. Hydrol. Process. 32 (13), 2058–2068. https://doi.org/10.1002/hyp.13137.

Bonneau, J., Fletcher, T.D., Costelloe, J.F., Burns, M.J., 2017. Stormwater infiltration and the 'urban karst'–A review. J. Hydrol. 552, 141–150. https://doi.org/10.1016/j.jhydrol.2017.06.043.

Braud, I., Breil, P., Thollet, F., Lagouy, M., Branger, F., Jacqueminet, C., Kermadi, S., Michel, K., 2013. Evidence of the impact of urbanization on the hydrological regime of a medium-sized periurban catchment in France. J. Hydrol. 485, 5–23. https://doi.org/10.1016/j.jhydrol.2012.04.049.

Brunner, G.W., 2016. HEC-RAS River analysis system, 2D modeling user's manual version 5.0. Davis: US Army Corps of Engineers, hydrologic engineering center.

Choat, B.E., Bhaskar, A.S., 2020. Spatial Arrangement of Stormwater Infiltration Affects Subsurface Storage and Baseflow. J. Hydrol. Eng. 25 (11), 04020048. https://doi.org/10.1061/(ASCE)HE.1943-5584.0002005.

Chow, V.T., 1959. Open-Channel Hydraulics. MCGraw-Hill, New York, 680 pp.

Chui, T.F.M., Freyberg, D.L., 2009. Implementing hydrologic boundary conditions in a multiphysics model. J. Hydrol. Eng. 14 (12), 1374–1377. https://doi.org/10.1061/(ASCE)HE.1943-5584.0000113.

Chui, T.F.M., Liu, X., Zhan, W., 2016. Assessing cost-effectiveness of specific LID practice designs in response to large storm events. J. Hydrol. 533, 353–364. https://doi.org/10.1016/j.jhydrol.2015.12.011.

Chui, T.F.M., Trinh, D.H., 2016. Modelling infiltration enhancement in a tropical urban catchment for improved stormwater management. Hydrol. Process. 30 (23), 4405–4419. https://doi.org/10.1002/hyp.10926.

City of Milwaukee, 2019. City of Mikwaukee - Green Infrastructure Plan.

City of Seattle, 2015. Green Stormwater Infrastructure in Seattle. Implementation Strategy 2015–2020.

Davies, J.P., Clarke, B.A., Whiter, J.T., Cunningham, R., 2001. Factors influencing the structural deterioration and collapse of rigid sewer pipes. Urban Water 3, 73–89. https://doi.org/10.1016/S1462-0758(01)00017-6.

Dewitz, J., 2019. National Land Cover Database (NLCD) 2016 Products: U.S. Geological Survey data release, https://doi.org/10.5066/P96HHBIE.

Downer, C.W., Ogden, F.L., 2006. Gridded surface subsurface hydrological analysis (GSSHA) user's manual; version 1.43 for watershed modeling system 6.1.

Ebrahimian, A., Wadzuk, B., Traver, R., 2019. Evapotranspiration in green stormwater infrastructure systems. Sci. Total Environ. 688, 797–810. https://doi.org/10.1016/j.scitotenv.2019.06.256.

Eger, C.G., Chandler, D.G., Driscoll, C.T., 2017. Hydrologic processes that govern stormwater infrastructure behaviour. Hydrol. Process. 31 (25), 4492–4506. https://doi.org/10.1002/hyp.11353.

Eiswirth, M., Houtzl, H., 2006. The impact of leaking sewers on urban groundwater. Groundwater Urban Environ. 1, 399–404.

Elachachi, S.M., Breysse, D., Denis, A., 2012. The effects of soil spatial variability on the reliability of rigid buried pipes. Comput. Geotech. 43, 61–71. https://doi.org/10.1016/j.compgeo.2012.02.008.

Ellis, B.M., Bertrand-Krajewski, J.L., 2010. Assessing infiltration and exfiltration on the performance of urban sewer systems. IWA Publishing.

Endreny, T., Collins, V., 2009. Implications of bioretention basin spatial arrangements on stormwater recharge and groundwater mounding. Ecol. Eng. 35 (5), 670–677. https://doi.org/10.1016/j.ecoleng.2008.10.017.

Fletcher, T.D., Shuster, W., Hunt, W.F., Ashley, R., Butler, D., Arthur, S., Trowsdale, S., Barraud, S., Semadeni-Davies, A., Bertrand-Krajewski, J.-L., Mikkelsen, P.S., Rivard, G., Uhl, M., Dagenais, D., Viklander, M., 2015. SUDS, LID, BMPs, WSUD and more–The evolution and application of terminology surrounding urban drainage. Urban Water J. 12 (7), 525–542.

Fry, T.J., Maxwell, R.M., 2017. Evaluation of distributed BMP s in an urban watershed—High resolution modeling for stormwater management. Hydrol. Process. 31 (15), 2700–2712. https://doi.org/10.1002/hyp.11177.

Fung, A., Babcock, R., 2020. A Flow-Calibrated method to project groundwater infiltration into coastal sewers affected by sea level rise. Water 12 (7), 1934. https://doi.org/10.3390/w12071934.

Ghodsi, S.H., Zhu, Z., Gheith, H., Rabideau, A.J., Torres, M.N., Meindl, K., 2021. Modeling the Effectiveness of Rain Barrels, Cisterns, and Downspout Disconnections for Reducing Combined Sewer Overflows in a City-Scale Watershed. Water Resour. Manage. 35 (9), 2895–2908.

Göbel, P., Stubbe, H., Weinert, M., Zimmermann, J., Fach, S., Dierkes, C., Kories, H., Messer, J., Mertsch, V., Geiger, W.F., Coldewey, W.G., 2004. Near-natural stormwater management and its effects on the water budget and groundwater surface in urban areas taking account of the hydrogeological conditions. J. Hydrol. 299 (3–4), 267–283. https://doi.org/10.1016/j.jhydrol.2004.08.013.

Golden, H.E., Hoghooghi, N., 2018. Green infrastructure and its catchment-scale effects: an emerging science. *Wiley Interdiscip*. Rev. Water 5 (1), e1254. https://doi.org/10.1002/wat2.1254.

Han, S., Song, H., 2017. Evaluation of Defect Types for Characteristic Database Construction of Large Sewage Box Culverts. J. Korean Soc. Water Wastewater 31 (6), 619–628. https://doi.org/10.11001/jksww.2017.31.6.619.

Harris, I., Osborn, T.J., Jones, P., Lister, D., 2020. Version 4 of the CRU TS monthly high-resolution gridded multivariate climate dataset. Sci. Data 7 (1), 1–18. https://doi.org/10.1038/s41597-020-0453-3.

Herrmann, D.L., Schifman, L.A., Shuster, W.D., 2018. Widespread loss of intermediate soil horizons in urban landscapes. Proc. Natl. Acad. Sci. U.S.A. 115 (26), 6751–6755. https://doi.org/10.1073/pnas.1800305115.

Jackson, R.B., Canadell, J., Ehleringer, J.R., Mooney, H.A., Sala, O.E., Schulze, E.D., 1996. A global analysis of root distributions for terrestrial biomes. Oecologia 108 (3), 389–411. https://doi.org/10.1007/BF00333714.

Jean, M.È., Duchesne, S., Pelletier, G., Pleau, M., 2018. Selection of rainfall information as input data for the design of combined sewer overflow solutions. J. Hydrol. 565, 559–569. https://doi.org/10.1016/j.jhydrol.2018.08.064.

Jiang, A.Z., McBean, E.A., Binns, A., Gharabaghi, B., 2019. Quantifying Rainfall-Derived Inflow from Private Foundation Drains in Sanitary Sewers: Case Study in London, Ontario, Canada. J. Hydrol. Eng. 24 (9), 05019023. https://doi.org/10.1061/(ASCE)HE.1943-5584.0001814.

Karpf, C., Franz, T., Krebs, P., 2007. Fractionation of infiltration and inflow (I/I) in urban sewer systems with regression analysis. NOVATECH 2007.

Karpf, C., Krebs, P., 2011. Quantification of groundwater infiltration and surface water inflows in urban sewer networks based on a multiple model approach. Water Res. 45 (10), 3129–3136. https://doi.org/10.1016/j.watres.2011.03.022.

Kaushal, S.S., Belt, K.T., 2012. The urban watershed continuum: evolving spatial and temporal dimensions. Urban Ecosyst. 15 (2), 409–435. https://doi.org/10.1007/s11252-012-0226-7.

Kousky, C., Olmstead, S.M., Walls, M.A., Macauley, M., 2013. Strategically placing green infrastructure: cost-effective land conservation in the floodplain. Environ. Sci. Technol. 47 (8), 3563–3570. https://doi.org/10.1021/es303938c.

Kracht, O., Gresch, M., Gujer, W., 2007. A stable isotope approach for the quantification of sewer infiltration. Environ. Sci. Technol. 41 (16), 5839–5845. https://doi.org/10.1021/es062960c.

Kracht, O., Gresch, M., Gujer, W., 2008. Innovative tracer methods for sewer infiltration monitoring. Urban Water J. 5 (3), 173–185. https://doi.org/10.1080/15730620802180802.

Lizárraga-Mendiola, L., Vázquez-Rodríguez, G.A., Lucho-Constantino, C.A., Bigurra-Alzati, C.A., Beltrán-Hernández, R.I., Ortiz-Hernández, J.E., López-León, L.D., 2017. Hydrological design of two low-impact development techniques in a semi-arid climate zone of central Mexico. Water 9 (8), 561. https://doi.org/10.3390/w9080561.

Lucas, W.C., Sample, D.J., 2015. Reducing combined sewer overflows by using outlet controls for Green Stormwater Infrastructure: Case study in Richmond, Virginia. J. Hydrol. 520, 473–488. https://doi.org/10.1016/j.jhydrol.2014.10.029.

Malek Mohammadi, M., Najafi, M., Kermanshachi, S., Kaushal, V., Serajiantehrani, R., 2020. Factors Influencing the Condition of Sewer Pipes: State-of-the-Art Review. J. Pipeline Syst. Eng. 11 (4), 03120002. https://doi.org/10.1061/(ASCE)PS.1949-1204.0000483.

Maxwell, R.M., Miller, N.L., 2005. Development of a coupled land surface and groundwater model. J. Hydrometeorol. 6 (3), 233–247. https://doi.org/10.1175/JHM422.1.

Mikalson, D., Guo, Y., Adams, B.J., 2012. Rainfall Derived Inflow and Infiltration Modeling Approaches. J. Water Manage. Model. R245–R308. https://doi.org/10.14796/JWMM.R245-08.

New York City Department of Environmental Protection (NYCDEP), 2012. NYC Green Infrastructure Plan: A Sustainable Strategy for Clean Waterways. New York City.

Nordman, E.E., Isely, E., Isely, P., Denning, R., 2018. Benefit-cost analysis of stormwater green infrastructure practices for Grand Rapids, Michigan, USA. J. Clean. Prod. 200, 501–510. https://doi.org/10.1016/j.jclepro.2018.07.152.

Okwori, E., Viklander, M., Hedström, A., 2021. Spatial heterogeneity assessment of factors affecting sewer pipe blockages and predictions. Water Res. 194, 116934. https://doi.org/10.1016/j.watres.2021.116934.

Pangle, L.A., Diem, J.E., Milligan, R., Adams, E., Murray, A., 2022. Contextualizing Inflow and Infiltration Within the Streamflow Regime of Urban Watersheds. e2021WR030406 Water Resour. Res. 58 (1). https://doi.org/10.1029/2021WR030406.

Pawlowski, C.W., Rhea, L., Shuster, W.D., Barden, G., 2014. Some factors affecting inflow and infiltration from residential sources in a core urban area: case study in a Columbus, Ohio, Neighborhood. J. Hydraul. Eng. 140 (1), 105–114. https://doi.org/10.1061/(ASCE)HY.1943-7900.0000799.

Peche, A., Graf, T., Fuchs, L., Neuweiler, I., 2017. A coupled approach for the three-dimensional simulation of pipe leakage in variably saturated soil. J. Hydrol. 555, 569–585. https://doi.org/10.1016/j.jhydrol.2017.10.050.

Prigiobbe, V., Giulianelli, M., 2009. Quantification of sewer system infiltration using δ18O hydrograph separation. Water Sci. Technol. 60, 727–735. https://doi.org/10.2166/wst.2009.399.

Randrup, T.B., McPherson, E.G., Costello, L.R., 2001. Tree root intrusion in sewer systems: review of extent and costs. J. Infrastruct. Syst. 7 (1), 26–31. https://doi.org/10.1061/(ASCE)1076-0342(2001)7:1(26).

Sandoval, S., Torres, A., Pawlowsky-Reusing, E., Riechel, M., Caradot, N., 2013. The evaluation of rainfall influence on combined sewer overflows characteristics: the Berlin case study. Water Sci. Technol. 68 (12), 2683–2690. https://doi.org/10.2166/wst.2013.524.

Schaap, M.G., Leij, F.J., Van Genuchten, M.T., 2001. ROSETTA: A computer program for estimating soil hydraulic parameters with hierarchical pedotransfer functions. J. Hydrol. 251 (3–4), 163–176. https://doi.org/10.1016/S0022-1694(01)00466-8.

Selvakumar, A., Field, R., Burgess, E., Amick, R., 2004. Exfiltration in sanitary sewer systems in the US. Urban Water J. 1 (3), 227–234. https://doi.org/10.1080/15730620410001732017.

Sohn, W., Kim, J.H., Li, M.H., Brown, R., 2019. The influence of climate on the effectiveness of low impact development: A systematic review. J. Environ. Manage. 236, 365–379. https://doi.org/10.1016/j.jenvman.2018.11.041.

Stewart, R.D., Lee, J.G., Shuster, W.D., Darner, R.A., 2017. Modelling hydrological response to a fully-monitored urban bioretention cell. Hydrol. Process. 31 (26), 4626–4638. https://doi.org/10.1002/hyp.11386.

Sun, G., Noormets, A., Chen, J., McNulty, S.G., 2008. Evapotranspiration estimates from eddy covariance towers and hydrologic modeling in managed forests in Northern Wisconsin, USA. Agric. For. Meteorol. 148 (2), 257–267. https://doi.org/10.1016/j.agrformet.2007.08.010.

Tan, P., Zhou, Y., Zhang, Y., Zhu, D.Z., Zhang, T., 2019. Assessment and pathway determination for rainfall-derived inflow and infiltration in sanitary systems: a case study. Urban Water J. 16 (8), 600–607. https://doi.org/10.1080/1573062X.2019.1700289.

Van Genuchten, M.T., 1980. A closed-form equation for predicting the hydraulic conductivity of unsaturated soils. Soil Sci. Soc. Am. J. 44 (5), 892–898. https://doi.org/10.2136/sssaj1980.03615995004400050002x.

Torres, M.N., Rodríguez, J.P., Leitão, J.P., 2017. Geostatistical analysis to identify characteristics involved in sewer pipes and urban tree interactions. Urban For. Urban Green. 25, 36–42. https://doi.org/10.1016/j.ufug.2017.04.013.

U.S. Geological Survey (USGS), 2016. National Water Information System data available on the World Wide Web (USGS Water Data for the Nation), accessed [Nov 4, 2020], at URL [http://waterdata.usgs.gov/nwis/].

Voter, C.B., Loheide, S.P., 2018. Urban residential surface and subsurface hydrology: synergistic effects of low-impact features at the parcel scale. Water Resour. Res. 54 (10), 8216–8233. https://doi.org/10.1029/2018WR022534.

Voter, C.B., Loheide, S.P., 2021. Climatic controls on the hydrologic effects of urban low impact development practices. Environ. Res. Lett. 16 (6), 064021.

Weill, S., Mouche, E., Patin, J., 2009. A generalized Richards equation for surface/subsurface flow modelling. J. Hydrol. 366 (1–4), 9–20. https://doi.org/10.1016/j.jhydrol.2008.12.007.

Weiss, G., Brombach, H., Haller, B., 2002. Infiltration and inflow in combined sewer systems: long-term analysis. Water Sci. Technol. 45 (7), 11–19. https://doi.org/10.2166/wst.2002.0112.

Wisconsin Department of Natural Resources (DNR), 2019. Wisconsin DEM and Hillshade from LiDAR. Published in January 2019. https://data-wi-dnr.opendata.arcgis.com/maps/wi-dnr::wisconsin-dem-and-hillshade-from-lidar-web-map/about.

Wisconsin Department of Natural Resources (DNR), 2020. The Bureau for Remediation and Redevelopment Tracking System (BRRTS) on the Web (BOTW). https://dnr.wisconsin.gov/topic/Brownfields/botw.html.

Wright, L.T., Dent, S., Mosley, C., Kadota, P., Djebbar, Y., 2001. Comparing rainfall dependent inflow and infiltration simulation methods. J. Water Manage. Model. https://doi.org/10.14796/JWMM.R207-16.

Zhang, K., Chui, T.F.M., 2017. Evaluating hydrologic performance of bioretention cells in shallow groundwater. Hydrol. Process. 31 (23), 4122–4135. https://doi.org/10.1002/hyp.11308.

Zhang, K., Chui, T.F.M., 2019. A review on implementing infiltration-based green infrastructure in shallow groundwater environments: Challenges, approaches, and progress. J. Hydrol. 579, 124089. https://doi.org/10.1016/j.jhydrol.2019.124089.

Zhang, K., Chui, T.F.M., 2020. Assessing the impact of spatial allocation of bioretention cells on shallow groundwater–An integrated surface-subsurface catchment-scale analysis with SWMM-MODFLOW. J. Hydrol. 586, 124910. https://doi.org/10.1016/j.jhydrol.2020.124910.

Zhang, Z., 2007. Estimating rain derived inflow and infiltration for rainfalls of varying characteristics. J. Hydraul. Eng. 133 (1), 98–105. https://doi.org/10.1061/(ASCE)0733-9429(2007)133:1(98).

Zhu, Y., Ishikawa, T., Subramanian, S.S., 2020. Simulation of runoff and infiltration using iterative cross-coupled surface and subsurface flows. Jpn. Geotech. Soc. Spec. Publ. 8 (3), 41–46. https://doi.org/10.3208/jgssp.v08.j13.